

Vortex-induced vibrations of a one-degree-of-freedom cylinder transitioning from the inline to the crossflow degree of freedom

Bridget M. Benner and Yahya Modarres-Sadeghi ^{*}

Department of Mechanical and Industrial Engineering, University of Massachusetts, Amherst, Massachusetts 01003, USA

 (Received 22 April 2021; accepted 28 September 2021; published 2 November 2021)

We have studied vortex-induced vibrations (VIV) of a flexibly mounted cylinder with one degree of freedom for different angles that the direction of oscillations makes with the incoming flow, covering the entire range from a purely inline direction ($\alpha = 0^\circ$) to a purely crossflow (transverse) direction ($\alpha = 90^\circ$). Force and displacement measurements together with flow visualizations of the wake are used to characterize the response of the cylinder over a range of reduced velocities ($1 < U^* < 14$). It is shown that the two lock-in ranges that are observed in a purely inline VIV response of the cylinder persist to higher angles: The first lock-in range, which corresponds to a symmetric or alternating-symmetric wake, persists up to $\alpha = 40^\circ$, and the second one up to $\alpha = 50^\circ$. The response of the system follows that of a purely inline case both quantitatively and qualitatively up to $\alpha = 15^\circ$, a relatively large deviation from the pure inline direction. The lock-in range, which is typically observed in a purely crossflow VIV response, appears at angles as low as $\alpha = 25^\circ$. For $\alpha > 50^\circ$, this crossflow-induced VIV response is the only response that is observed. It is also shown that the symmetric and alternating-symmetric wakes that had been observed previously in a purely inline case are observed for angles up to $\alpha = 30^\circ$ and $\alpha = 15^\circ$, respectively, indicating that their formation does not rely on a perfect alignment between the direction of oscillations and the flow direction. For larger angles, a skewed symmetric shedding is observed in which one of the two vortices that are shed simultaneously is larger than the other one.

DOI: [10.1103/PhysRevFluids.6.114702](https://doi.org/10.1103/PhysRevFluids.6.114702)

I. INTRODUCTION

When a bluff body with a circular cross section is placed in flow, beyond a critical Reynolds number, vortices are shed in its wake [1,2]. The shedding frequency of these vortices increases linearly with the incoming flow velocity following the Strouhal law [2]. If the cylinder is free to oscillate, then oscillations are observed when the shedding frequency and the natural frequency of the structure become equal. These oscillations are called vortex-induced vibrations (VIV).

The majority of previous studies on VIV have been on a cylinder free to oscillate in the direction perpendicular to the direction of the incoming flow [transverse or crossflow (CF) direction] [3–5]. In these cases, a range of relatively large amplitude oscillations, with amplitudes of up to around one cylinder diameter, are observed for a range of reduced velocities (a dimensionless flow velocity defined as $U^* = U/f_{nw}D$, where U is the flow velocity, f_{nw} is the structure's natural frequency in otherwise still fluid, and D is the cylinder's diameter). These oscillations start at $U^* \sim 5$, and extend to reduced velocities of $U^* \sim 8 - 12$, or even larger, depending on the system's mass ratio [5], defined as $m^* = m/m_d$, where m is the cylinder's mass and m_d is the mass of displaced fluid.

^{*}modarres@engin.umass.edu

If the cylinder is free to oscillate only in the direction of the incoming flow [inline (IL) direction], then IL VIV is observed [6–13]. In these cases, the response consists of two regions of nonzero amplitude oscillations as the reduced velocity is increased, both of which occur at lower reduced velocities compared with the range of oscillations in the CF direction. The first range of oscillations is observed at a range of $U^* \sim 1.7 - 2.5$, and the second range of oscillations is observed at a range of $U^* \sim 2.75 - 4$. The amplitudes of these oscillations are much smaller than those in the CF VIV, reaching values of less than $0.1D$. The first range of oscillations is observed only if the system is disturbed externally by giving nonzero initial conditions to the cylinder. These oscillations result in a symmetric shedding of the vortices in the wake, where two vortices of the same size are shed simultaneously from the two sides of the cylinder during each cycle of oscillations. Recently, an alternating-symmetric wake was observed toward the end of this first region of oscillations in which, while a pair of symmetric vortices is shed in the wake in each cycle of oscillations, the relative size of these vortices alternates, resulting in the shedding of a larger vortex from one side in one cycle followed by a larger vortex from the other side in the next cycle [13]. The oscillations of the second region in a pure IL direction are due to the synchronization between the fluctuating forces in the IL direction and the system's natural frequency. Since the fluctuating forces are at two times the shedding frequency in the IL direction, this synchronization occurs at a reduced velocity of approximately half of that for the onset of oscillations in the CF direction. The wake in the second region is an asymmetric wake, where one vortex is shed from each side of the cylinder in each cycle of oscillations.

Clearly there are differences both in the ranges of observed oscillations in the CF and IL directions and the observed vortices in their wakes. Oscillations in the IL direction occur at lower reduced velocities compared with the CF direction. Symmetric and alternating-symmetric wakes are observed only in the IL direction, and not in the CF direction. The questions then arise such as how far one can deviate from the inline direction while still observing symmetric and alternating-symmetric shedding. Will these types of shedding be observed only when the direction of the cylinder's oscillations is perfectly aligned with the incoming flow or will they survive despite a slight deviation from the perfect alignment? How much deviation from the inline direction will result in the disappearance of the two ranges of oscillations that are observed in a pure IL direction? Will the first range of oscillations together with its symmetric wake exist if the cylinder is placed at an angle slightly different from zero? Or will it disappear with the slightest misalignment? What will happen to the second region of nonzero amplitudes observed in the IL VIV response? Will it also disappear as the angle of the degree of freedom deviates from zero slightly, or will it exist for higher angles? Thinking about the CF VIV response, how far can one deviate from the transverse direction for the oscillations that are observed in the CF direction to disappear? Will a slight deviation from the 90° angle result in a dramatic change in the width of the lock-in range and the amplitudes of the observed oscillations? Also, will there be an angle for which we observe both the IL-induced and CF-induced oscillations with three regions of nonzero amplitude oscillations? Besides their relevance to the fundamental research, these questions are important from an applied point of view. For instance, when a system undergoes VIV, if the direction of the incoming flow changes (i.e., due to the change in the wind direction or the current direction for ocean structures) will the VIV response of the system be affected significantly? Clearly this will have implications in proper estimations of fatigue life of such systems [14–16].

This problem has received very limited attention in the past. Ongoren and Rockwell [17] conducted a series of experiments on a cylinder forced to move sinusoidally at different angles with respect to the incoming flow and investigated the different types of modes of vortex formation. Bourguet [18] conducted a numerical study at a Reynolds number of $Re = 100$ with the goal of investigating the influence of imposed rotation on the response of a cylinder free to oscillate at an arbitrary angle with respect to the incoming flow. Bourguet [18] also ran a set of simulations on a cylinder with no rotation. Due to the low Reynolds number used in these simulations, the oscillations in the IL direction were of negligible amplitudes. Bourguet observed that as the angle was increased, oscillations started at a reduced velocity range corresponding to the range for which oscillations in

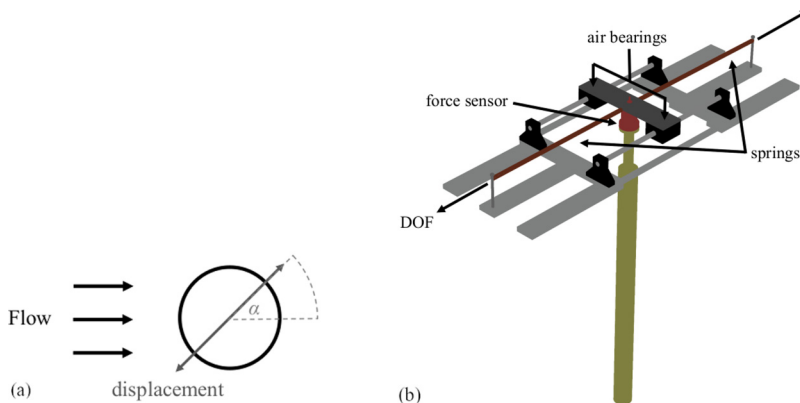


FIG. 1. (a) The direction of the cylinder oscillations with respect to the direction of incoming flow at angle α , and (b) a schematic of the experimental setup.

a purely CF system are observed. The width of the lock-in range and the amplitude of oscillations increased as the angle was increased, and the maximum amplitude was observed for the case where the cylinder was free to oscillate in the CF direction.

Here, we present the results of a series of experiments we have conducted on a one-degree-of-freedom flexibly mounted cylinder placed in flow in which we varied the angle that the direction of oscillations makes with the direction of the incoming flow from $\alpha = 0^\circ$ (for the purely inline case) to $\alpha = 90^\circ$ (for the purely CF direction). In these experiments, we measured the cylinder's oscillations and the flow forces that act on it during these oscillations, and at the same time we conducted flow visualizations of the wake to answer the questions that we have listed above.

II. EXPERIMENTAL SETUP AND MEASUREMENT TECHNIQUES

A. Experimental setup

The experiments were conducted in a recirculating water tunnel, with a test section of $1.27 \text{ m} \times 0.5 \text{ m} \times 0.38 \text{ m}$ and a turbulence intensity of less than 1% for a flow velocity of up to $U = 0.3 \text{ m/s}$. Two circular cylinders were used: one hollow aluminum cylinder that was used for $\alpha \leq 55^\circ$ to cover the entire IL-induced VIV response range, and one acrylic cylinder that was used for $\alpha \geq 40^\circ$ to cover higher angles at larger reduced velocities. The first cylinder had a diameter of $D = 25.4 \text{ mm}$ and was submerged in flow by a length of $L = 355 \text{ mm}$ which corresponded to an aspect ratio of $\epsilon = 14$. The cylinder was comprised of a hollow aluminum tube with a wall thickness of 1.59 mm and acrylonitrile butadiene styrene (ABS) plastic printed parts consisting of an endcap and cylindrical extension that interfaced with the force sensor. Waterproof epoxy was used to join the hollow aluminum tube and ABS plastic printed parts to ensure the cylinder was sealed. The second cylinder was made of acrylic and had the same diameter as the hollow aluminum cylinder, $D_{\text{acrylic}} = 25.4 \text{ mm}$, and its submerged length was $L_{\text{acrylic}} = 280 \text{ mm}$, corresponding to an aspect ratio of $\epsilon_{\text{acrylic}} = 11$. The acrylic cylinder was used for $\alpha \geq 40^\circ$ because the ABS plastic cylindrical extension affixed to the hollow aluminum cylinder could not withstand the flow forces at higher reduced velocities for which oscillations were observed for larger values of α . ABS plastic was chosen for the cylindrical extension for the aluminum cylinder setup to reduce the moving mass of the system for lower angles, for which mainly IL oscillations were expected. The experiments at $\alpha = 40^\circ$ were conducted using both cylinders to ensure that no significant change is observed due to the use of two different cylinders. Each cylinder was mounted on low-damping air bearings that allowed for one degree of freedom. Springs extended from the metal plate (atop the air bearings) to a fixed mounting point (Fig. 1). This air bearing setup and hollow cylinder were used before for other

IL VIV studies [13]. The mass ratio was $m^* = m/\rho V_d = 1.5$ for the hollow aluminum cylinder and $m^* = 2.6$ for the acrylic cylinder, where m is the total moving mass of the system (including the cylinder, air bearings, mounting plate, force sensor, and various cabling), ρ is the density of water, and V_d is the volume of the submerged cylinder.

B. Displacement and force measurements

Flow forces acting on the cylinder were measured using an ATI-Nano17/IP68 six-axis force sensor that was mounted to the cylindrical attachment affixed to the cylinder. Displacement of the cylinder was measured using a Micro-Epsilon ILD 1402-600 noncontacting displacement sensor for a duration of 60s, once the system reached steady state, for each data point. Force and displacement measurements were taken for varying angles in the range of $0^\circ < \alpha < 90^\circ$ over a reduced velocity range of $1.0 < U^* < 14$, which correspond to a Reynolds number range of $700 < Re < 10300$. To change the angle at which the circular cylinder could freely move with respect to the flow [Fig. 1(a)], the entire setup [Fig. 1(b)] was incrementally rotated to the desired angle. The reported angles are accurate within $\pm 0.2^\circ$. Decay tests were conducted in air and water by giving the cylinder an initial displacement and recording the response. The natural frequencies of the cylinders in water and in air were found using decay tests to be $f_{nw} \sim 1.19$ Hz and $f_{na} \sim 1.56$ Hz for the hollow aluminum cylinder, and $f_{nw} \sim 1.14$ Hz and $f_{na} \sim 1.35$ Hz for the acrylic cylinder. The corresponding structural damping ratio was found to be $\zeta = 0.003$ for both cylinders, resulting in a mass-damping coefficient of $m^*\zeta = 0.005$ for the hollow aluminum cylinder and $m^*\zeta = 0.008$ for the acrylic cylinder. For all experiments, the water level was held constant and the flow velocity was increased in increments of ~ 2.5 mm/s to cover the reduced velocity range tested.

C. Flow visualization

Flow visualization tests were conducted using hydrogen bubbles to study the vortex shedding patterns in the wake of the cylinder. The system used for hydrogen bubble generation has been used before by the authors [19,20]. Hydrogen bubbles were generated through electrolysis of water by which a negatively charged platinum-iridium wire with a diameter of 0.0508 mm acted as the anode and a positively charged graphite plate acted as the cathode. The wire was strung upstream from the structure across the test section perpendicular to the flow and the graphite plate was placed upstream from the platinum wire parallel to the flow. The potential difference between the charged wire and graphite plate caused a buildup of hydrogen bubbles along the platinum wire which, once separated from the wire, created a bubble plane used to view the wake structure. The wake images were captured using a Phantom Miro M110 high-speed camera placed underneath the test section.

III. AMPLITUDE RESPONSE

The amplitude response of the cylinder for small angles, i.e., those close to the IL direction, is shown in Fig. 2(a), where the dimensionless amplitude, $A^* = A/D$ (in which A is the oscillation amplitude), is plotted versus the reduced velocity. The purely inline case, $\alpha = 0^\circ$, serves as a reference for all angled cases. Similar to the previous studies on purely IL VIV [7–13], the response for $\alpha = 0^\circ$ in the present study exhibits two regions of nonzero amplitudes, with maximum amplitudes of around $0.1D$. The width of the two regions of nonzero oscillations are also similar to what has been observed in the past [13]: In the present study, two regions of nonzero amplitudes are observed for reduced velocity ranges of $1.6 < U^* < 2.4$ and $2.7 < U^* < 3.6$, in agreement with what Gurian *et al.* observed [13], except that in their case, the second region was extended to a slightly larger reduced velocity of $U^* = 3.8$. This slight difference is mainly due to minor differences in the experimental setups as well as experimental error. Also, similar to previous studies, the response at reduced velocities between the two oscillation regions is not at zero amplitude, but a very small amplitude compared with the two oscillation regions. The oscillation magnitudes are larger in

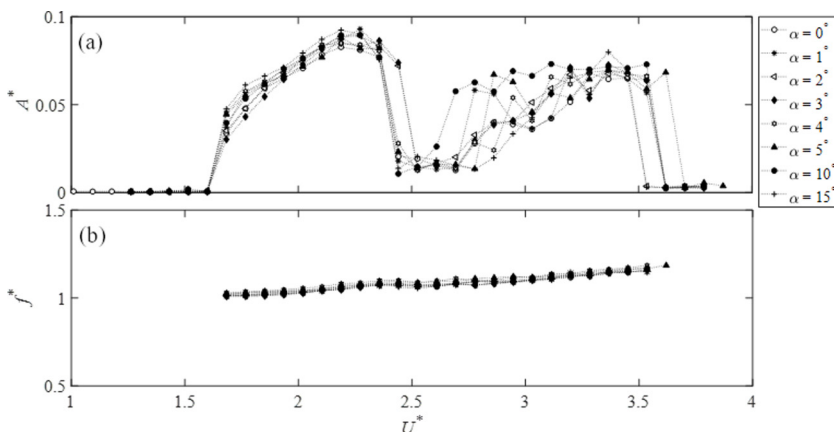


FIG. 2. (a) Dimensionless amplitude and (b) dimensionless oscillation frequency versus reduced velocity for $0^\circ < \alpha < 15^\circ$. These results are obtained using the hollow aluminum cylinder.

the first region of VIV compared with the second region. The maximum oscillation magnitude is $A^* = 0.08$ at $U^* = 2.2$ in the first VIV region and $A^* = 0.07$ at $U^* = 3.3$ in the second VIV region.

The results shown in Fig. 2(a) include angles from 1° to 5° in increments of 1° , and angles from 5° to 15° in increments of 5° . The smaller angles, $\alpha = 1^\circ - 5^\circ$, represent slight deviations from the pure IL direction, such as those that could occur in an experimental study, where one aims at aligning the direction of motion with the direction of the incoming flow perfectly, but fails due to possible experimental errors. The larger angles, $\alpha = 5^\circ - 15^\circ$, represent cases of more significant, and perhaps intentional, deviations from the pure IL direction. The results of Fig. 2(a) show that the amplitude response of the cylinder is very similar to the response of the cylinder in the purely inline case ($\alpha = 0^\circ$) for all of these angles. Also shown in Fig. 2(b) are the corresponding oscillation frequencies normalized by the natural frequency of the system in water, f^* , for all reduced velocities where oscillations are observed. All dimensionless oscillation frequencies remain close to 1, which indicates that the oscillation frequency has locked in with the structure's natural frequency and thus the cylinder is experiencing VIV. Clearly, for a deviation of up to 15° from the IL direction, neither the ranges of reduced velocities for which oscillations are observed nor the amplitudes of these oscillations are affected by the imposed asymmetry in the system. The scatter that is observed at the beginning of the second oscillation region, $2.6 < U^* < 3$, is most probably due to the type of shedding that is observed in this region. It is shown that for $\alpha = 0^\circ$, a competitive shedding occurs in this region, in which two wake modes, symmetric and asymmetric, compete with one another. This competition between two wake modes could be responsible for the fluctuations in the response over this range.

At $\alpha = 20^\circ$ [Fig. 3(a)], the width of the first nonzero amplitude region decreases slightly: This range starts at the same reduced velocity as that for the smaller angles, but ends at a slightly smaller reduced velocity. The width of the first nonzero amplitude region continues to decrease as the angle is increased further ($\alpha > 20^\circ$), until the first lock-in range collapses at $\alpha = 45^\circ$ [Fig. 3(c)]. Large amplitude oscillations (relative to the magnitude of oscillations for the purely inline case) are observed in the second VIV region until these oscillations collapse at $\alpha = 55^\circ$ [Fig. 3(d)]. This transition of the response from the two nonzero amplitude regions to no oscillations in this range of reduced velocities, as α is increased, is more clearly observed in the three-dimensional plot of Fig. 4. For reduced velocities toward the end of the second nonzero amplitude region for $25^\circ < \alpha < 50^\circ$, the oscillations are observed to go to zero amplitude for some reduced velocities and then go back to nonzero amplitudes as the reduced velocity is increased, creating amplitude spikes in Fig. 4.

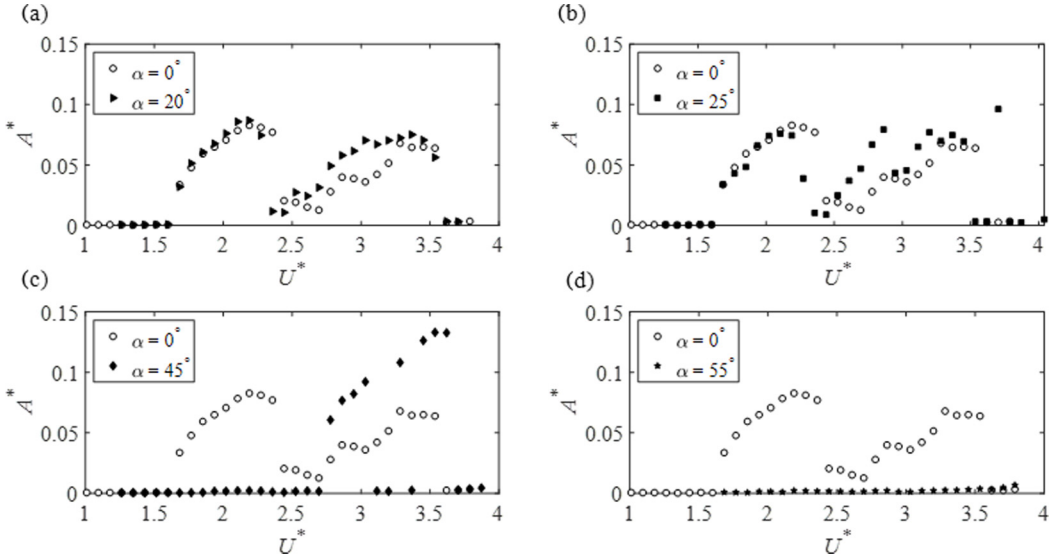


FIG. 3. Dimensionless amplitude of oscillations A^* versus reduced velocity U^* for (a) $\alpha = 20^\circ$, (b) $\alpha = 25^\circ$, (c) $\alpha = 45^\circ$, and (d) $\alpha = 55^\circ$. In all cases $\alpha = 0^\circ$ is given as a reference. These results are obtained using the hollow aluminum cylinder.

Based on Fig. 4, it is clear that the overall IL VIV behavior, i.e., the two lock-in regions, are observed up to an angle of $\alpha = 40^\circ$. Despite this significant asymmetry in the system, the response resembles that of purely IL oscillations, with quantitative differences in the amplitude of oscillations and the exact width of the lock-in regions. For angles $45^\circ \leq \alpha \leq 50^\circ$, while the first region of the IL VIV response has disappeared, the second region still persists.

Signs of CF VIV start appearing at larger reduced velocities for angles as low as $\alpha = 25^\circ$ (Fig. 5). At $\alpha = 25^\circ$, oscillations with very small amplitudes ($A^* \sim 0.03$) are observed within a reduced velocity range over which CF VIV is expected for a purely CF system [Fig. 5(a)]. The amplitudes of these oscillations at $\alpha = 25^\circ$ are very small—much smaller than what would resemble any VIV-type response. However, as the angle is increased slightly, i.e., by 5° , clear nonzero amplitude regions, resembling the VIV response of a CF VIV case, are observed starting at $\alpha = 30^\circ$.

Figure 5(a) shows the dimensionless amplitudes of oscillations versus the reduced velocity for all angles where the third VIV range is observed. The blue markers represent results based on the

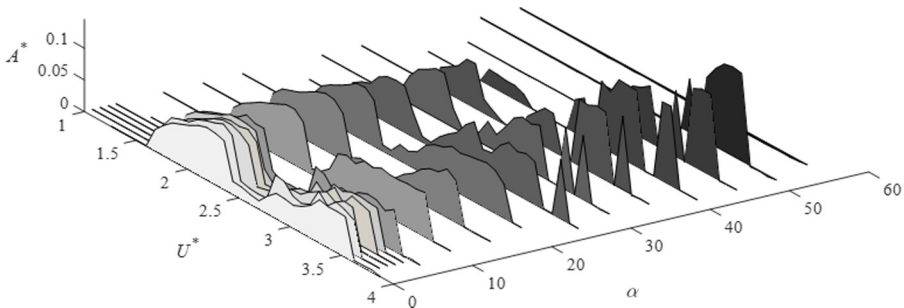


FIG. 4. Three-dimensional plot of the dimensionless amplitude of oscillations A^* versus the reduced velocity U^* for angles in the range of $0^\circ \leq \alpha \leq 55^\circ$. These results are obtained using the hollow aluminum cylinder.

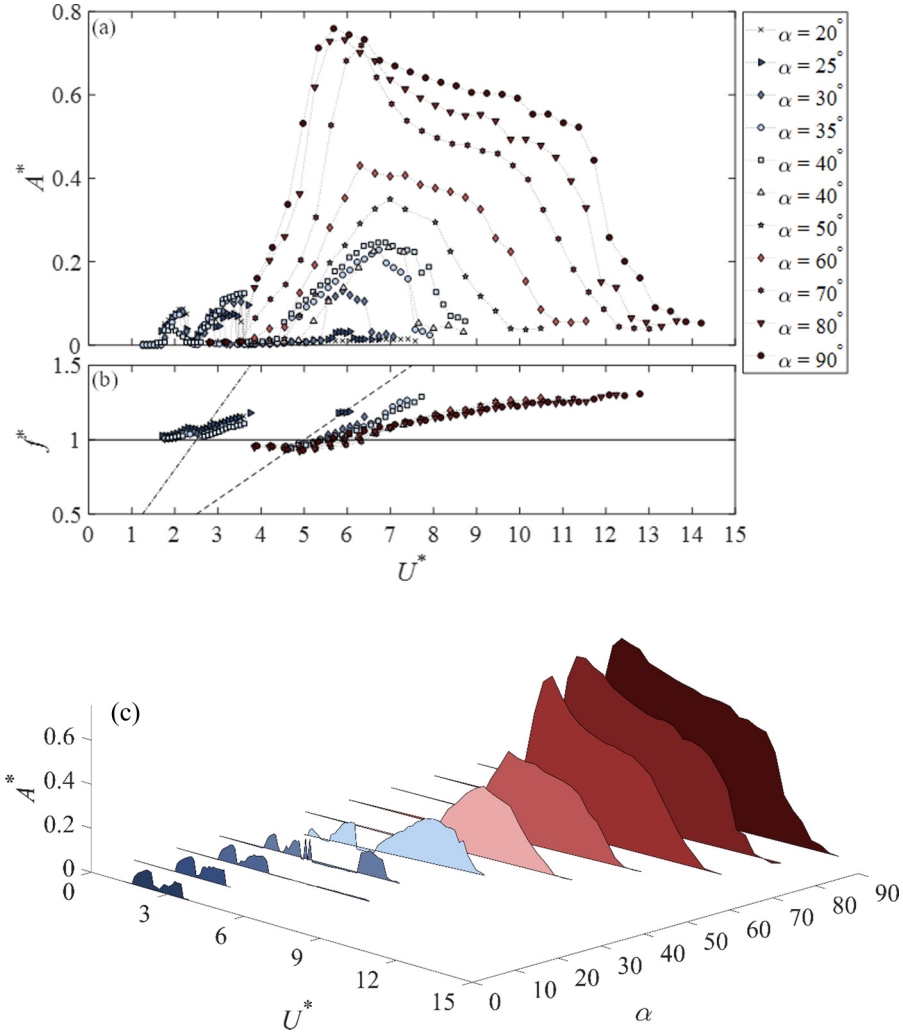


FIG. 5. (a) Dimensionless amplitude of oscillations A^* and (b) dimensionless frequency f^* versus reduced velocity U^* for the hollow aluminum cylinder at $\alpha = 20^\circ\text{--}40^\circ$ (blue markers) and the acrylic cylinder at $\alpha = 40^\circ\text{--}90^\circ$ (red markers), together with (c) a 3D representation of the amplitude of oscillations A^* at different angles.

hollow aluminum cylinder ($\alpha = 20^\circ\text{--}40^\circ$) and the red markers represent results based on the acrylic cylinder ($\alpha = 40^\circ\text{--}90^\circ$). Since the hollow aluminum cylinder was replaced with the acrylic cylinder at $\alpha = 40^\circ$, amplitude values for both the aluminum (blue square markers) and acrylic (red triangle markers) cylinders are shown at this angle. The amplitude values for the acrylic cylinder are slightly smaller than the amplitude values for the aluminum cylinder because the mass-damping coefficient is greater for the acrylic cylinder setup compared with the aluminum cylinder setup. The difference in the mass-damping coefficient also impacts the lock-in range for both series of experiments at $\alpha = 40^\circ$, whereby the lock-in range is slightly wider for the aluminum cylinder setup (which has a lower mass-damping coefficient) as compared with the acrylic cylinder setup.

It is seen in Fig. 5 that as α is increased, the width of the third lock-in range and the maximum amplitude of oscillations in that region increase as well. The lock-in range reaches a range of $U^* = 4 - 13$ at $\alpha = 90^\circ$ with a maximum amplitude of $A^* \sim 0.8$. For the pure CF case, both the

upper branch and the lower branch have been observed with their corresponding maximum amplitudes of $A^* = 0.8$ and 0.6 , respectively, which are very close to values shown by Williamson and Govardhan [5] for a system with $(m^* + C_A)\zeta = 0.011$. The upper branch has been observed also for lower angles of $\alpha = 70^\circ$ and 80° , with almost the same maximum amplitude as $\alpha = 90^\circ$, but it disappears at $\alpha = 60^\circ$. As α is decreased, the width of the lock-in range and the maximum amplitude of oscillations within the lock-in range decrease. The decrease in the width of the lock-in range is observed mainly as a sooner end of the synchronization. The peak amplitude moves to higher reduced velocities as α is decreased, except for the smallest angles for which this lock-in range has been observed: $\alpha = 25^\circ$ and 30° . A major drop in the maximum amplitude is observed between $\alpha = 70^\circ$ and $\alpha = 60^\circ$, where maximum amplitude drops from $A^* \sim 0.7$ to $A^* \sim 0.4$, due to the disappearance of the upper branch at $\alpha = 60^\circ$.

The corresponding dimensionless oscillation frequency plots of Fig. 5(b) clearly show two different regions of synchronizations: one corresponding to the lock-in due to IL synchronization, and one corresponding to the lock-in due to the CF synchronization. Two lines, corresponding to the shedding frequency and two times the shedding frequency, estimated based on the Strouhal law are also plotted in the figure. The first region's synchronization is with two times the shedding frequency, since oscillations that are observed in this region are due to the IL synchronization that occurs when the natural frequency of the system equals two times the shedding frequency, since the fluctuating force frequency in the inline direction is two times the shedding frequency. This first region corresponds to both nonzero amplitude oscillation regions observed in the lower reduced velocity cases, and the range of almost (but not completely) zero amplitude oscillations in between those two regions. As the reduced velocity is increased, oscillations are observed at higher reduced velocities, which correspond to a synchronization between the shedding frequency and the natural frequency, and those are the oscillations that resemble the typical CF VIV response. For both ranges, the oscillation frequency increases with increasing reduced velocity.

The plot of Fig. 5(c) gives an overall view of the cylinder's response at different angles. Besides giving a clear comparison among the relative amplitudes of oscillations at different angles and at different reduced velocities, this plot shows that at lower angles, only the lock-in ranges due to the IL synchronization exist. Then as the angle is increased, for $\alpha = 30^\circ$ to $\alpha = 40^\circ$, all three lock-in ranges exist in the cylinder's response, and for higher angles, $\alpha > 50^\circ$, the lock-in range due to the CF synchronization is the only observed VIV response. Note that at $\alpha = 50^\circ$, Fig. 5(c) shows only the response of the cylinder at higher reduced velocities (based on the data from the acrylic cylinder), and does not include the second IL lock-in region that is observed at lower reduced velocities with the hollow cylinder.

The results of Fig. 5 can also shed light on what is observed in the VIV of a two degree of freedom (2DOF) system, in which a cylinder is free to oscillate in both the IL and CF directions. When in a 2DOF system, the natural frequencies in the CF and IL directions are identical (e.g., [7]) as the reduced velocity is increased from zero, lock-in in the IL direction occurs first, and IL oscillations are observed, and CF oscillations start at higher reduced velocities where lock-in occurs in the CF direction. This corresponds to what is observed in the plots of Fig. 5: The purely IL lock-in starts earlier than the CF lock-in. If, however, in a 2DOF system, the ratios of the IL and CF natural frequencies are set to be equal to 2 [21–23], dual resonance can occur, in which the CF and the IL lock-in occur at the same time, since due to the 2:1 ratio between the IL and CF natural frequencies, the forcing frequency is equal to both natural frequencies at the same reduced velocity. With a 2:1 ratio between the natural frequencies, the amplitude plot for the purely IL angle in Fig. 5 would have shifted to values of reduced velocity twice as large as their present values, and the onset of lock-in in both purely IL and purely CF directions would have been at the same value of reduced velocity.

IV. WAKE STRUCTURES AND FLOW FORCES FOR LOWER ANGLES

Four different shedding patterns have been observed in the literature for a circular cylinder undergoing inline VIV [13]. We have also observed these four patterns in the wake of our purely inline case, i.e., $\alpha = 0^\circ$, as shown in the first row of Fig. 6. At the beginning of the first lock-in range, a symmetric shedding is observed in which two vortices of the same size are shed simultaneously from the two sides of the cylinder in each cycle of oscillations [e.g., at $U^* = 1.9$, Fig. 6(a)]. Toward the end of the first lock-in range, alternating-symmetric (AS) shedding is observed in which, while again two vortices are shed from the two sides of the cylinder simultaneously during each cycle of oscillations, the relative sizes of these vortices alternate in each cycle [e.g., at $U^* = 2.2$, Fig. 6(b)]. For the range of almost-zero-amplitude response between the two lock-in ranges, a competitive shedding is observed in which symmetric and asymmetric shedding patterns coexist [e.g., at $U^* = 2.8$, Fig. 6(c)]. In the second IL lock-in range, an asymmetric shedding is observed in which two single vortices are shed from the two sides of the cylinder, one after the other, in each cycle of oscillations [e.g., at $U^* = 3.3$, Fig. 6(d)]. Here, we consider four reduced velocities within these four regions with distinct shedding patterns, and we will discuss how these patterns change as α is increased. Besides the shedding patterns, we will present the frequencies of the fluctuating flow forces (normalized by the natural frequency in water) acting on the cylinder in the direction of oscillations and perpendicular to it. These forces provide insight into the symmetry or asymmetry of the shedding patterns at any given reduced velocity. A summary of how the force coefficients in the x and y directions change versus the reduced velocity and for various angles is given in Fig. 7. Forces are greater in the direction of displacement (x direction), compared with the direction perpendicular to displacement (y direction), for lower reduced velocities ($U^* < 2.5$), and smaller for higher reduced velocities. This is consistent with the shedding patterns observed for each α case, as the cylinder transitions from symmetric shedding to asymmetric shedding as the reduced velocity is increased. We discuss in detail how these wake structures and flow forces relate to one another in what follows.

A. Symmetric shedding—sample case $U^* = 1.9$

The observed wake during the major part of the first lock-in range in a purely IL VIV case, $\alpha = 0^\circ$, is a symmetric shedding in which one pair of symmetric vortices of opposite signs is shed per oscillation cycle. This pattern is observed here for the pure IL case as well, as an example, at $U^* = 1.9$ [Fig. 6(a)]. As α is increased, this symmetric shedding wake pattern is observed for all angles up to $\alpha = 40^\circ$ [Figs. 6(e), 6(i), 6(m), and 6(q)], and they only disappear when the first VIV region collapses at $\alpha = 45^\circ$ [Fig. 6(u)]. There are slight changes in the symmetric shedding as the angle is increased. For $\alpha = 0^\circ$, the frequency contents of the flow forces are consistent with symmetric shedding since one peak is observed in the direction of displacement, x , which matches the natural frequency of the system [Fig. 8]. The fluctuating forces acting perpendicular to the direction of motion, i.e., in the y direction, are negligible since two vortices of opposite signs are shed simultaneously from both sides of the cylinder and cancel the forces exerted from each side. As α is increased, the peak frequency remains to be the frequency in the x direction; however, small contributions at $f^* = 0.5$ are observed in the y -direction force frequency contents starting at $\alpha = 35^\circ$ [Fig. 8]. These small values are due to the slight differences in the size of vortex pairs that are shed in each cycle of oscillations. Starting at $\alpha = 35^\circ$, a skewed symmetric shedding pattern is observed in which the vortex that is shed from the lower side of the cylinder is always slightly larger than the vortex that is shed from its upper side. At $\alpha = 40^\circ$ the oscillations of the cylinder are very small, and the shedding of vortices occurs farther downstream relative to the smaller angles as shown in Fig. 6(q). When the first VIV region collapses at $\alpha = 45^\circ$, the shear layers do not interact with each other until much farther downstream [Fig. 6(u)] and do not impart forces that cause the cylinder to oscillate.

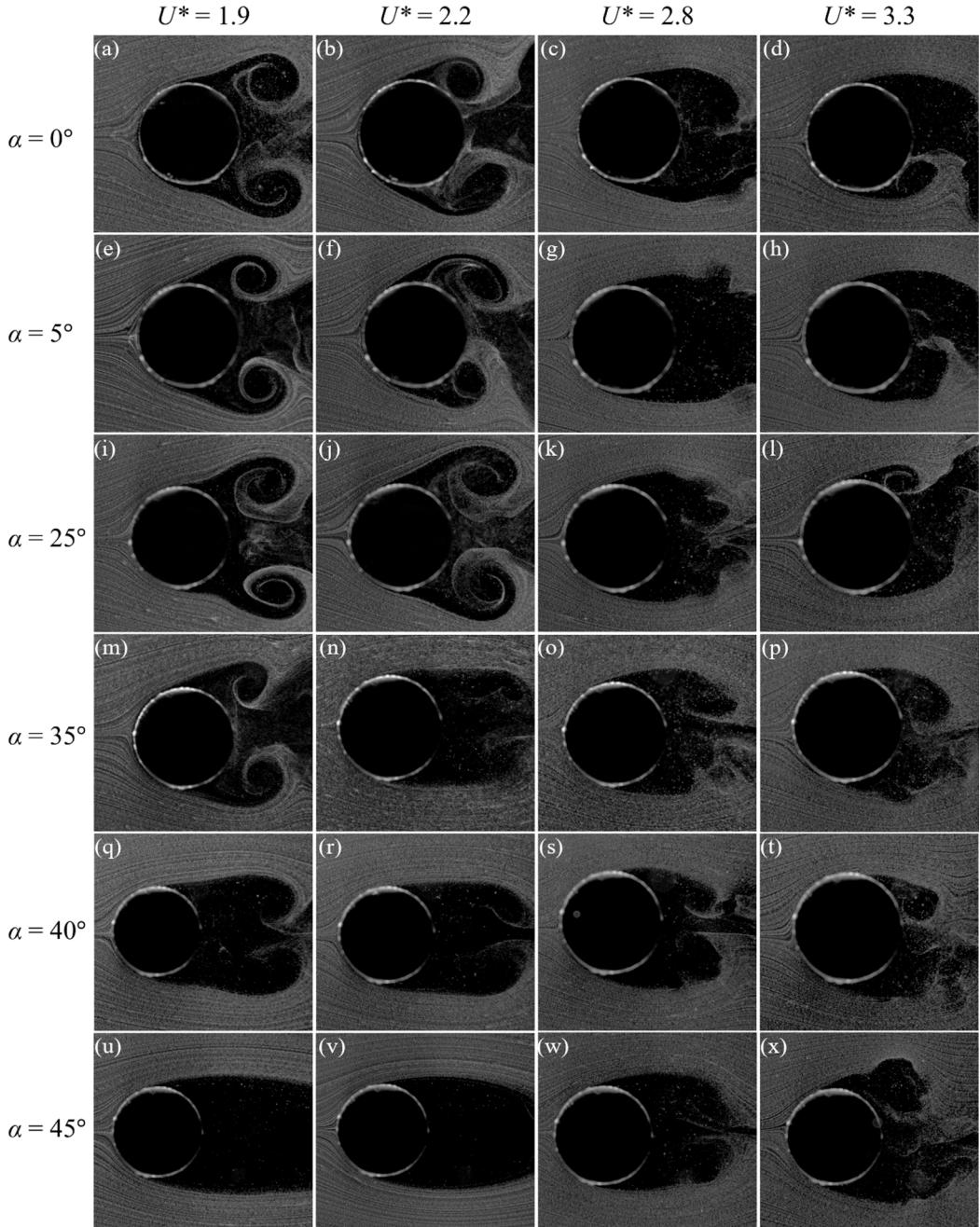


FIG. 6. Flow visualizations of the wake as the angle is increased for sample reduced velocities for which a purely IL case exhibits a symmetric wake ($U^* = 1.9$, first column from the left), alternating-symmetric wake ($U^* = 2.2$, second column), competitive wake ($U^* = 2.8$, third column), and asymmetric wake ($U^* = 3.3$, fourth column).

B. Alternating-symmetric (AS) shedding—sample case $U^* = 2.2$

Toward the end of the first lock-in region, e.g., at $U^* = 2.2$, the cylinder exhibits AS shedding in the purely inline direction where two unequal-sized vortices are shed simultaneously per oscillation

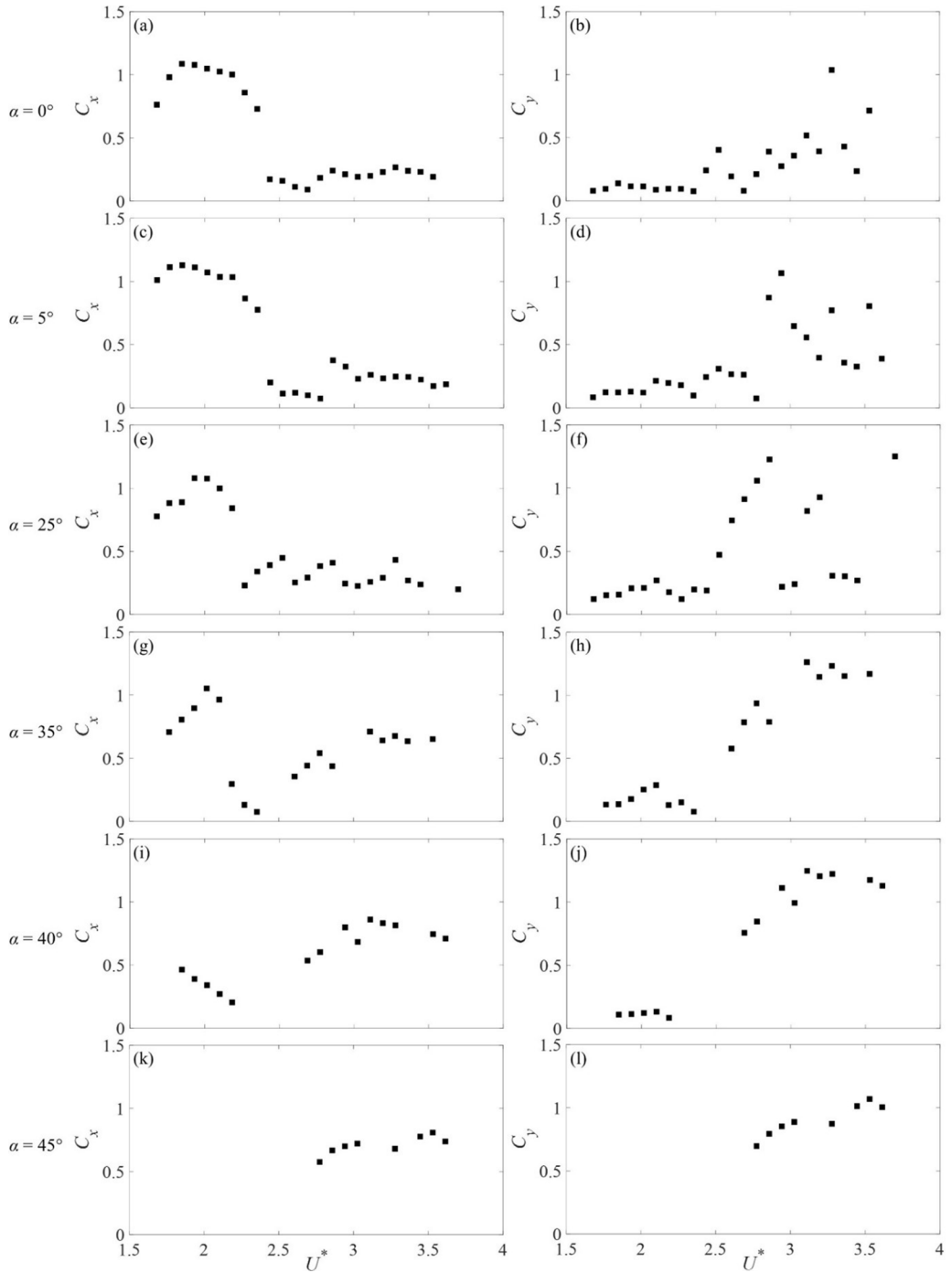


FIG. 7. Force coefficients in the x (C_x) and y (C_y) directions versus the reduced velocity at $\alpha = 0^\circ, 5^\circ, 25^\circ, 35^\circ, 40^\circ$, and 45° .

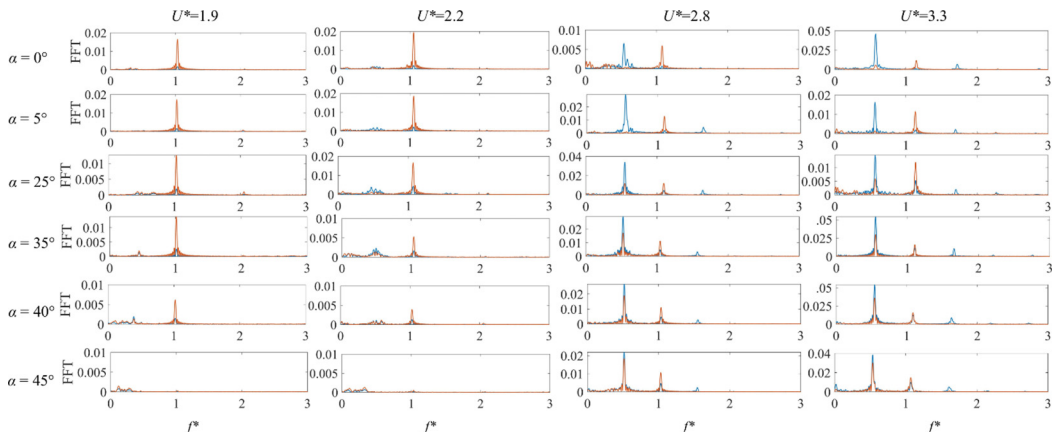


FIG. 8. Frequency contents of forces in the direction of displacement (x , red) and perpendicular to the displacement (y , blue) at $\alpha = 0^\circ, 5^\circ, 25^\circ, 35^\circ, 40^\circ$, and 45° for $U^* = 1.9, 2.2, 2.8$, and 3.3 .

cycle and alternate in size for each cycle [Fig. 6(b)]. This shedding pattern was identified and classified by Gurian *et al.* [13]. In the present study, this shedding pattern is observed beyond the purely inline case. The snapshots of Fig. 9 show that the AS shedding exists for both $\alpha = 0^\circ$ and $\alpha = 5^\circ$. In our visualizations, we observed the AS shedding for up to $\alpha = 15^\circ$. The shedding pattern transitions at $\alpha = 20^\circ$ at which point again skewed symmetric shedding is observed. In the skewed shedding patterns, the vortex that is shed from the side that is in the direction of the cylinder's oscillations is always slightly larger than the other vortex.

The oscillation magnitudes and fluctuating flow forces at $U^* = 2.2$ are larger than the previous case, $U^* = 1.9$, for the smaller angles ($\alpha = 0^\circ, 5^\circ, 25^\circ$). Fluctuating flow forces acting in the y direction are no longer negligible, although the fluctuating forces in the x direction are still much larger and are the dominant forces driving the motion of the cylinder. The frequency contents of the fluctuating flow forces show a peak frequency in the x direction at $f^* = 1$, where the response frequency matches the natural frequency of the system, similar to the previous reduced velocity case. However, a small frequency peak at half the natural frequency of the system, $f^* = 0.5$, now emerges in the y direction for all of the smaller angle cases, i.e., $\alpha = 0^\circ, 5^\circ, 25^\circ$ (second column of Fig. 8). This is due to a slight asymmetry that is introduced to the system by the AS shedding pattern. At $\alpha = 35^\circ$ and 40° , the cylinder experiences small-amplitude oscillations and small fluctuating forces (relative to smaller angles at the same reduced velocity) are observed to act on the cylinder and frequency contributions from the crossflow forces are more apparent at $f^* = 0.5$ for both the x and y directions, at these higher angles (Fig. 8).

A measure of asymmetry in the wake, as defined by Gurian *et al.* [13], is the ratio of the fluctuating lift to the fluctuating drag force R_f : For a perfectly symmetric shedding, this ratio is zero, as the fluctuating lift force is zero. As the asymmetry in the wake is increased, R_f increases. Figure 10 shows how R_f changes as the angle is increased for the two sample reduced velocities that correspond to the symmetric and alternating-symmetric wakes, at $U^* = 1.9$ and 2.2 , respectively. For a symmetric shedding, R_f stays smaller than 0.05 for angles of up to $\alpha = 30^\circ$, and increases only slightly for $\alpha = 35^\circ$ and more significantly for $\alpha = 40^\circ$ when differences in the size of the shed vortices are observed. For the AS wakes, R_f remains at values smaller than 0.1 for up to $\alpha = 15^\circ$, for which we have observed AS wake in our visualizations, and then increases to values close to 0.25 for $\alpha = 20^\circ$ – 30° , and to 0.6 for $\alpha = 35^\circ$ – 40° . This increase of R_f to relatively larger values is an indication of disappearance of the AS wake for these angles, as also observed in the wake visualizations.

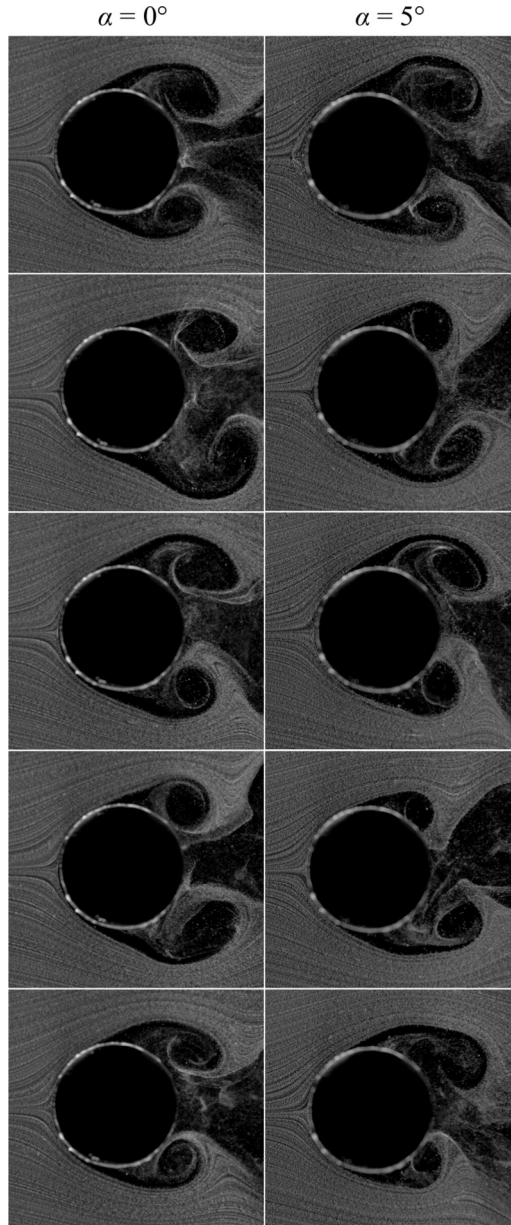


FIG. 9. Snapshots of alternating-symmetric wake for $\alpha = 0^\circ$ and 5° at $U^* = 2.2$.

C. Competitive shedding—sample case $U^* = 2.8$

At an even higher reduced velocity, e.g., $U^* = 2.8$, weak and competitive shedding is observed in the purely in-line direction, where the wake structure resembles both symmetric and asymmetric shedding patterns and is essentially indistinguishable. This shedding pattern remains consistent as the angle at which the cylinder is free to oscillate is increased (Fig. 6), but the response of the cylinder changes. At lower angles ($\alpha = 0^\circ$ and 5°), the cylinder is between the two VIV regions and exhibits very small oscillation magnitudes as shown in Fig. 2(a). The corresponding fluctuating flow forces in both the x and y directions are also very small. The frequency contents of the fluctuating

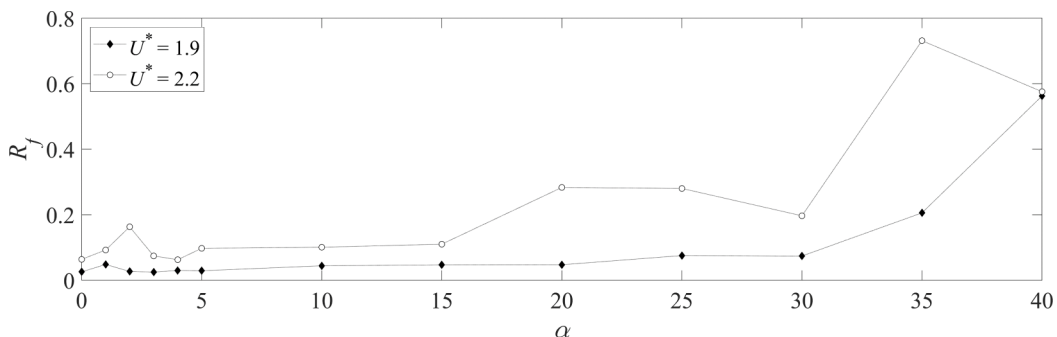


FIG. 10. The ratio of the fluctuating lift and fluctuating drag R_f versus α for symmetric ($U^* = 1.9$) and alternating-symmetric ($U^* = 2.2$) wakes.

flow forces acting in the x direction drive the motion of the cylinder, but the magnitude of the fluctuating flow forces in the y direction at $f^* = 0.5$ is now larger than the previous two cases ($U^* = 1.9$ and 2.2) as shown in Fig. 8. As the degree of freedom is positioned at higher angles with respect to the incoming flow, $\alpha = 25^\circ$, 35° , 40° , and 45° , the magnitude of the fluctuating flow forces at $f^* = 0.5$ in the y direction increases as shown in Fig. 8, highlighting the increased asymmetry in the system, and the appearance of asymmetric shedding in the wake. At nonzero angles, signs of contributions of higher harmonics of the flow forces in the y direction appear as a small peak at three times the peak frequency, i.e., $f^* = 3 \times 0.5 = 1.5$. These third harmonic contributions have been observed in the past in the VIV response of a cylinder in the CF direction, and are due to the fact that the motions at an angle with respect to the incoming flow are due to the combination of the fluctuating lift and fluctuating drag forces, which act at frequencies equal to the shedding frequency and twice the shedding frequency, respectively, resulting in a three times the shedding frequency component if superimposed in a direction other than the purely IL and CF directions.

D. Asymmetric shedding—sample case $U^* = 3.3$

Within the second VIV region, e.g., at $U^* = 3.3$, asymmetric shedding is observed for the purely inline case where two vortices are shed from each side of the cylinder, one after the other, per oscillation cycle. The shedding pattern remains consistent at this reduced velocity for angles that deviate from the purely inline case (Fig. 6) until the second VIV branch collapses at $\alpha = 55^\circ$. The frequency contents of the fluctuating flow forces also remain consistent as the angle is increased (Fig. 8). The frequency contents are in agreement with the shedding pattern observed. A well-defined peak at $f^* = 0.5$ is observed in the y direction, while a frequency peak that matches the natural frequency of the system is observed in the x direction. The frequency contents of the fluctuating flow forces imply that the shedding frequency is equal to $f_{nw}/2$ and that two vortices are shed from opposite sides of the cylinder per cycle of shedding. The third-harmonic component that appeared in the competitive region at $f^* = 1.5$ exists in this asymmetric shedding region as well (Fig. 8). The fluctuating flow forces increase in magnitude as α is increased. At higher angles, $\alpha = 35^\circ$, 40° , and 45° , high-amplitude oscillations that correspond to large fluctuating flow forces are observed.

E. Overview of flow force frequencies

An overview of the fluctuating flow force frequencies (normalized by the natural frequency of the structure in otherwise still water) versus the reduced velocity for smaller angles ($\alpha = 0^\circ$, 5° , 25° , 35° , 40° , 45°) is given in Fig. 11. For the purely inline case, $\alpha = 0^\circ$, a peak at $f^* \sim 1$ (the same as what was observed in Fig. 2 for the displacement) is observed in the x direction, for all reduced velocities

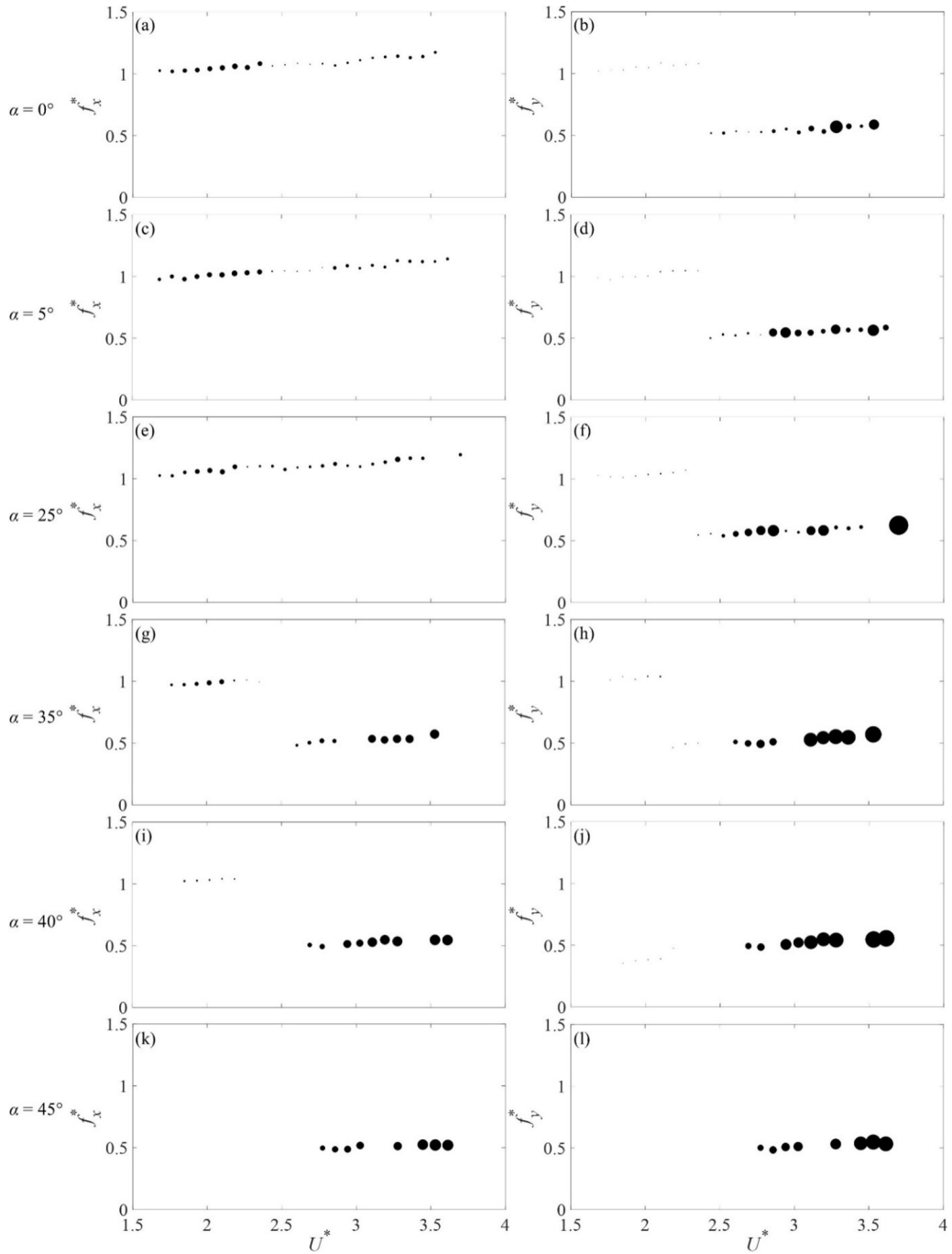


FIG. 11. Frequency contents of the flow forces in the x direction (left column), and in the y direction (right column) versus reduced velocity for different angles. The symbol size is proportional to the strength of the frequency.

for which the structure was observed to oscillate. This observation is indicative of synchronization between the oscillation frequency and force frequency and confirms that the observed oscillations are indeed VIV. As α is increased, $f^* \sim 1$ remains the most pronounced frequency, and due to the asymmetry of the system, a contribution at $f^* \sim 0.5$ appears in the force frequencies in the x direction at higher reduced velocities in the second VIV region for $\alpha = 35^\circ$ and increases in strength as the angle is increased.

For the lower reduced velocities of the first VIV region, the frequency contents of the fluctuating forces in the x direction have a dominant frequency equal to $f^* \sim 1$ while the frequency contents of the fluctuating forces in the y direction are negligible for smaller reduced velocities for all sample cases shown. This is consistent with the symmetric shedding pattern that is observed for smaller reduced velocities since one peak is observed in the direction of displacement that matches the natural frequency of the system. At the tail end of the first VIV region, $f^* \sim 1$ in the x direction remains the driving force of the motion, but a small frequency peak at half the natural frequency of the system, $f^* \sim 0.5$, emerges in the y direction for the smaller angle cases ($\alpha = 0^\circ, 5^\circ, 25^\circ$). This indicates a slight asymmetry that is introduced to the system as the wake structure transitions from symmetric shedding to an alternating-symmetric shedding pattern.

At higher reduced velocities, within the second VIV region, the frequency contents of the fluctuating flow forces exhibit a dominant frequency in the x direction at $f^* \sim 1$, similar to the trend observed in the first VIV region. At higher angles, $f^* = 0.5$ becomes the dominant frequency in the x direction. Frequency contents of the fluctuating flow forces in the y direction increase in strength, compared with the first VIV region, at $f^* \sim 0.5$.

V. CONCLUSIONS

The response of a low-mass-damping cylinder placed in flow and allowed to oscillate in one degree of freedom at varying angles with respect to the incoming flow, $0^\circ \leq \alpha \leq 90^\circ$, over a range of reduced velocities of $1.0 < U^* < 14$, was studied experimentally. The angle at which the cylinder was allowed to oscillate was incrementally varied to capture the response of the cylinder as it transitioned from the purely streamwise to the purely crossflow direction. Flow force and displacement measurements were conducted in tandem with flow visualizations to quantify the changes in the cylinder response as the angle was varied.

The response of the cylinder in the purely streamwise direction, $\alpha = 0^\circ$, was consistent with what has been observed in previous studies [12,13] in that two regions of VIV responses are observed at relatively low reduced velocities. The wake structure transitions as the reduced velocity is increased and ultimately four wake structures are observed: symmetric shedding, alternating-symmetric shedding, weak and competitive shedding, and asymmetric shedding. The frequency contents of the displacement and flow force measurements confirm that VIV occurs at all reduced velocities where oscillations are observed, because the peak oscillation frequencies and force frequencies in the direction of motion were synchronized. At lower reduced velocities, when symmetric shedding occurs in the wake of the cylinder, the peak flow force frequency in the direction of motion (the streamwise direction) is at $f^* = 1$ and the flow force frequencies in the direction perpendicular to the direction of motion (the crossflow direction) are negligible. As the reduced velocity is increased, and the wake structure transitions to alternating-symmetric shedding in the wake of the cylinder, a small frequency peak at half the natural frequency of the system, $f_{nw}/2$, emerges in the direction perpendicular to the direction of motion which indicates a slight asymmetry in the system. As the reduced velocity is increased further, and the wake structure transitions to asymmetric shedding, the peak at half the natural frequency of the system, $f_{nw}/2$, in the direction perpendicular to the direction of oscillations becomes the dominant frequency since two vortices are shed from opposite sides of the cylinder per shedding cycle.

At slightly higher angles, $1^\circ \leq \alpha \leq 15^\circ$, the amplitudes of oscillations and oscillation frequencies remain largely the same as the purely inline case, indicating that a deviation of up to 15° has minimal effect on the IL VIV response of a circular cylinder. At $\alpha = 20^\circ$, the width of the first lock-in region

decreases slightly. This trend continues as the angle of the degree of freedom is increased until the first lock-in region collapses at $\alpha = 45^\circ$. This again indicates that up to $\alpha = 40^\circ$, the main features of the pure IL VIV response are observed in the response of a cylinder that oscillates with a very large angle with respect to the purely in-line degree of freedom. Oscillations in the second lock-in region are observed up to $\alpha = 50^\circ$, and at $\alpha = 55^\circ$ the second lock-in region collapses. The first signs of the third lock-in region, consistent with the response of a circular cylinder placed in crossflow, emerges at higher reduced velocities for $\alpha = 25^\circ$. As α is increased further, the peak amplitude of oscillations and the width of the lock-in range increase and the largest peak amplitude and the widest lock-in range occur at $\alpha = 90^\circ$, the purely crossflow case.

The symmetric shedding that is observed in the wake of the cylinder within the first lock-in range of a purely IL case persists for up to $\alpha = 30^\circ$, and the alternating-symmetric shedding, which is observed toward the end of the first lock-in range, persists up to $\alpha = 15^\circ$, both of which were confirmed through flow visualization. For higher angles, a skewed symmetric shedding is observed within the first lock-in range, in which one of the two shed vortices is consistently larger than the other one. These observations were also confirmed by measuring the ratio between the fluctuating flow force in the y direction and the x direction, R_f , which stays very close to zero when the wake is symmetric.

These results exhibit that the response that is typically observed for a cylinder undergoing purely IL VIV is not sensitive to the exact alignment of the direction of motion and the direction of the incoming flow. A deviation of up to 15° has no quantitative or qualitative influence on the cylinder's response and its wake. This was to some extent surprising, especially considering that the symmetric and alternating-symmetric wakes that had been observed before for purely IL VIV cases intuitively seem to be very sensitive to this alignment. The qualitative behavior of the cylinder at lower reduced velocities resembles that of a purely IL case for up to 40° —a very large deviation from a pure IL case. The second IL lock-in range stays up to a very large angle of 50° . Signs of CF lock-in appear at 25° , and these oscillations slowly become the only response for angles larger than 50° . For a range of angles between 25° and 40° , the response consists of three lock-in ranges: two mainly IL lock-in ranges at the lower reduced velocities and one mainly CF lock-in range at higher reduced velocities.

-
- [1] C. Mathis, M. Provansal, and L. Boyer, The Benard-Von Karman instability: An experimental study near the threshold, *J. Phys., Lett.* **45**, 483 (1984).
 - [2] R. D. Blevins, *Vortex Induced Vibrations* (Van Nostrand Reinhold, New York, 1990).
 - [3] P. Bearman, Vortex shedding from oscillating bluff bodies, *Annu. Rev. Fluid Mech.* **16**, 195 (1984).
 - [4] T. Sarpkaya, A critical review of the intrinsic nature of vortex induced vibrations, *J. Fluid Struct.* **19**, 389 (2004).
 - [5] C. H. K. Williamson and R. Govardhan, Vortex-induced vibrations, *Annu. Rev. Fluid Mech.* **36**, 413 (2004).
 - [6] A. Okajima, T. Kosugi, and A. Nakamura, Flow-induced in-line oscillation of a circular cylinder in a water tunnel, *J. Pressure Vessel Technol.* **124**, 89 (2002).
 - [7] N. Jauvtis and C. H. K. Williamson, The effect of two degrees of freedom on vortex-induced vibration at low mass and damping, *J. Fluid Mech.* **509**, 23 (2004).
 - [8] N. Cagny and S. Balabani, On multiple manifestations of the second response branch in streamwise vortex-induced vibrations, *Phys. Fluids* **25**, 075110 (2013).
 - [9] N. Cagny and S. Balabani, Wake modes of a cylinder undergoing free streamwise vortex-induced vibrations, *J. Fluid Struct.* **38**, 127 (2013).
 - [10] N. Cagny and S. Balabani, Mode competition in streamwise-only vortex induced vibrations, *J. Fluid Struct.* **41**, 156 (2013).
 - [11] E. Konstantinidis, On the response and wake modes of a cylinder undergoing streamwise vortex-induced vibration, *J. Fluid Struct.* **45**, 256 (2014).

- [12] N. Cagney and S. Balabani, Streamwise vortex-induced vibrations of cylinders with one and two degrees of freedom, *J. Fluid Mech.* **758**, 702 (2014).
- [13] T. D. Gurian, T. Currier, and Y. Modarres-Sadeghi, Flow force measurements and the wake transition in purely inline vortex-induced vibration of a circular cylinder, *Phys. Rev. Fluids* **4**, 034701 (2019).
- [14] H. Mukundan, Y. Modarres-Sadeghi, J. M. Dahl, F. S. Hover, and M. S. Triantafyllou, Monitoring fatigue damage on marine risers, *J. Fluids Struct.* **25**, 617 (2009).
- [15] Y. Modarres-Sadeghi, H. Mukundan, J. M. Dahl, F. S. Hover, and M. S. Triantafyllou, The effect of higher harmonic forces on fatigue life of marine risers, *J. Sound Vib.* **329**, 43 (2010).
- [16] H. Zheng, R. E. Price, Y. Modarres-Sadeghi, and M. S. Triantafyllou, On fatigue damage of long flexible cylinders due to the higher harmonic force components and chaotic vortex-induced vibrations, *Ocean Eng.* **88**, 318 (2014).
- [17] A. Ongoren and D. Rockwell, Flow structure from an oscillating cylinder. Part 2. Mode competition in the near wake, *J. Fluid Mech.* **191**, 225 (1988).
- [18] R. Bourguet, Flow-induced vibrations of a rotating cylinder in an arbitrary direction, *J. Fluid Mech.* **860**, 739 (2019).
- [19] B. Seyed-Aghazadeh, D. W. Carlson, and Y. Modarres-Sadeghi, Vortex-induced vibration and galloping of prisms with triangular cross-sections placed in water flow, *J. Fluid Mech.* **817**, 590 (2017).
- [20] B. Benner, D. W. Carlson, B. Seyed-Aghazadeh, and Y. Modarres-Sadeghi, Vortex-induced vibration of symmetric airfoils used in vertical-axis wind turbines, *J. Fluids Struct.* **91**, 102577 (2019).
- [21] J. M. Dahl, F. S. Hover, and M. S. Triantafyllou, Resonant Vibrations of Bluff Bodies Cause Multi-Vortex Shedding and High Frequency Forces, *Phys. Rev. Lett.* **99**, 144503 (2007).
- [22] J. M. Dahl, F. S. Hover, M. S. Triantafyllou, and O. H. Oakley, Dual resonance in vortex-induced vibrations at subcritical and supercritical Reynolds numbers, *J. Fluid Mech.* **643**, 395 (2010).
- [23] D. W. Carlson, T. Currier, and Y. Modarres-Sadeghi, Flow-induced vibrations of a square prism free to oscillate in the crossflow and inline directions, *J. Fluid Mech.* **919**, A2 (2021).